Novel and Highly Potent ATR Inhibitor M4344 Kills Cancer Cells With Replication Stress, and Enhances the Chemotherapeutic Activity of Widely Used DNA Damaging Agents

Ukhyun Jo[1], Ilya S. Senatorov[2], Astrid Zimmermann[3], Liton Kumar Saha[1], Yasuhisa Murai[1], Se Hyun Kim[1,4], Vinodh N. Rajapakse[1], Fathi Elloumi[1,5], Nobuyuki Takahashi[1], Christopher W. Schultz[1], Anish Thomas[1], Frank T. Zenke[3], and Yves Pommier[1]

ABSTRACT

Although several ATR inhibitors are in development, there are unresolved questions regarding their differential potency, molecular signatures of patients with cancer for predicting activity, and most effective therapeutic combinations. Here, we elucidate how to improve ATR-based chemotherapy with the newly developed ATR inhibitor, M4344 using *in vitro* and *in vivo* models. The potency of M4344 was compared with the clinically developed ATR inhibitors BAY1895344, berzosertib, and ceralasertib. The anticancer activity of M4344 was investigated as monotherapy and combination with clinical DNA damaging agents in multiple cancer cell lines, patient-derived tumor organoids, and mouse xenograft models. We also elucidated the anticancer mechanisms and potential biomarkers for M4344. We demonstrate that M4344 is highly potent among the clinically developed ATR inhibitors. Replication stress (RepStress) and neuroendocrine (NE) gene expression signatures are significantly associated with a response to M4344 treatment. M4344 kills cancer cells by inducing cellular catastrophe and DNA damage. M4344 is highly synergistic with a broad range of DNA-targeting anticancer agents. It significantly synergizes with topotecan and irinotecan in patient-derived tumor organoids and xenograft models. Taken together, M4344 is a promising and highly potent ATR inhibitor. It enhances the activity of clinical DNA damaging agents commonly used in cancer treatment including topoisomerase inhibitors, gemcitabine, cisplatin, and talazoparib. RepStress and NE gene expression signatures can be exploited as predictive markers for M4344.

Introduction

DNA damage commonly occurs in all living cells and needs to be repaired to avoid genomic instability. DNA damage response (DDR) pathways coordinate the detection of cellular DNA damage and engage a molecular network required for cell-cycle adaptation and repair process to maintain cell viability (1, 2). Defects of DDR in cancer therapy with DNA-damaging agents are being exploited in the concept of synthetic lethality, providing treatment benefits for patients with cancer in terms of treatment selection and enhanced therapeutic response (3, 4). Major ongoing efforts in drug discovery are focused on small-molecule inhibitors of DDR activation caused by cellular oncogenic stress and DNA damaging agents (5, 6).

The cellular DDR pathways are primarily centered around three phosphatidylinositol 3-kinase like kinases (PIKKs): ataxia telangiectasia and rad3-related (ATR), ataxia telangiectasia mutated (ATM), and DNA-dependent protein kinase (DNA-PK/PRKDC) (7). ATR is the key kinase activated by replication stress among the three DDR kinases, which shares many substrates with ATM (8). Abnormal accumulation of single-stranded DNA coated by replication protein A (RPA) triggers the activation of ATR at the sites of replicative damage. Activated ATR phosphorylates checkpoint kinase 1 (CHK1), leading to cell-cycle arrest, pausing of DNA synthesis and initiation of DNA repair (9).

Given its pivotal role in replication stress-induced DDR activation, ATR is an attractive target for combination therapy with DNA-damaging agents (9, 10). Multiple clinical trials are ongoing with small-molecule ATR inhibitors (11, 12). Those studies consist of ATR inhibitors as monotherapy and in combination with DNA replication inhibitors (gemcitabine), topoisomerase inhibitors (topotecan, irinotecan), platinum derivatives, and poly (ADP-ribose) polymerase (PARP) inhibitors. Four ATR inhibitors, M4344 (VX-803), BAY1895344, berzosertib (M6620/VX-970), and ceralasertib (AZD6738; **Fig. 1A**) are in multiple clinical trials (13–16).

Phosphorylated CHK1 and phosphorylation of the Ser-139 residue of the histone variant H2AX (γH2AX) are established pharmacodynamic biomarkers in cancer therapy with ATR inhibition (17). Loss of ATM, inactivation of TP53, BRCA1/2, BRG1, ARID1A, and oncogenic activation of MYC and cyclin E (CCNE1) have been proposed to select patients for treatment with ATR inhibitors (18–21). However, additional reliable molecular biomarkers predicting sensitivity to ATR inhibitors are needed. Recently, several studies have used gene expression signatures of a specific

[1]Developmental Therapeutics Branch and Laboratory of Molecular Pharmacology, Center for Cancer Research, NCI, Bethesda, Maryland. [2]Laboratory of Genitourinary Cancer Pathogenesis, Center for Cancer Research, National Cancer Institute, Bethesda, Maryland. [3]Merck KGaA, Biopharma R&D, Translational Innovation Platform Oncology, Darmstadt, Germany. [4]Division of Hematology and Medical Oncology, Department of Internal Medicine, Seoul National University Bundang Hospital, Seongnam, Gyeonggi-do, South Korea. [5]General Dynamics Information Technology Inc., Fairfax, Virginia.

Note: Supplementary data for this article are available at Molecular Cancer Therapeutics Online (http://mct.aacrjournals.org/).

Y. Pommier is a lead contact.

Corresponding Authors: Ukhyun Jo and Yves Pommier, 37 Convent Dr., Building 37-Room 5068, Bethesda, MD 20892. Phone: 240-760-6142; Fax: 240-541-4475; E-mail: ukhyun.jo@nih.gov and pommier@nih.gov

Mol Cancer Ther 2021;20:1431–41

doi: 10.1158/1535-7163.MCT-20-1026

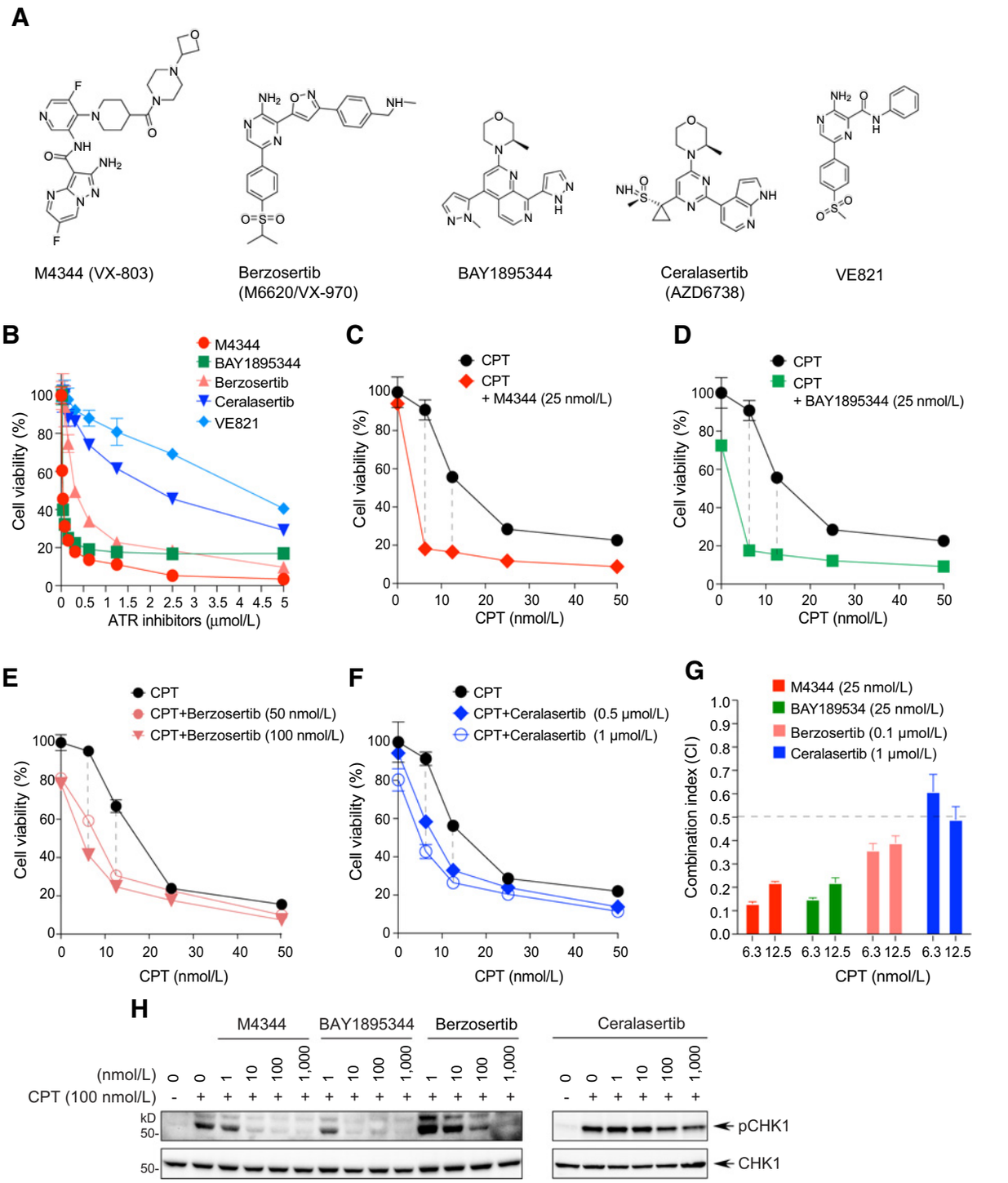

Figure 1.

Comparison between M4344 and other clinical ATR inhibitors. **A,** Chemical structures of ATR inhibitors. **B,** Comparative analysis of cell viability between clinical ATR inhibitors. DU145 cells were treated as indicated for 72 hours. Cell viability was accessed by CellTiter-Glo assay. **C–F,** Synergistic effects between ATR inhibitors and camptothecin (CPT). Cells were co-incubated with CPT (100 nmol/L) and M4344 (**C**), BAY1895344 (**D**), berzosertib (**E**), and ceralasertib (**F**) as indicated concentrations for 72 hours. Cell viability was accessed by CellTiter-Glo assay. **G,** Comparison of combination index values obtained for combination treatments of CPT (6.3 and 12.5 nmol/L) with the indicated ATR inhibitors. **H,** Inactivation of ATR-mediated CHK1 phosphorylation by ATR inhibitors. DU145 cells were pretreated with the indicated concentrations of ATR inhibitors for 1 hour and then incubated with CPT (100 nmol/L) and the ATR inhibitors for three additional hours. Protein levels were examined by Western blotting (see Supplementary Fig. S1 for effects of M4344 in H82 and U2OS cells).

cancer type or specific subtypes to determine a standard assessment for cancer therapy with novel diagnostic tools and therapeutic schemes (22–24). However, approaches to associate between gene expression signatures and the activity of ATR inhibitors have not yet been fully explored.

Although development of ATR inhibitors is active in clinic, ATR is essential for cell proliferation and biallelic loss of ATR gene function results in early embryonic lethality (25), emphasizing the needs for precision therapeutic strategies reducing side effects. Here, we first report that M4344 is a highly potent ATR inhibitor that enhances anticancer activity of clinical DNA damaging agents *in vitro* and *in vivo* models.

Materials and Methods

Cell lines and drugs

DU145 and U2OS cells were obtained from ATCC and cultured in DMEM media with 10% FBS and penicillin/streptomycin. H82, H446, H146, H209, A549, DMS114, SAOS-2, H1299, K562, HCT116, CCRF-CEM, MOLT-4, and SK-OV-3 cells were acquired from ATCC and grown in RPMI media with 10% FBS and penicillin/streptomycin. HAP-1 cells were purchased from Horizon Discovery and cultured in IMDM media with 10% FBS and penicillin/streptomycin. All cell lines were passaged 15 times and examined by MycoAlert Mycoplasma Detection Kit (Lonza).

M4344 and berzosertib were obtained from EMD Serono, Billerica, MA (a biopharmaceutical business of Merck KGaA, Darmstadt, Germany). Camptothecin, topotecan, LMP400, exatecan, SN-38, ceralasertib, VE-821, and BAY1895344 were acquired from the Developmental Therapeutics Program (DCTD, NCI). Etoposide (E1383) and cisplatin (P4394) were purchased from Millipore-Sigma. Talazoparib was provided by BioMarin Pharmaceutical Inc.

Cell viability assay

Cells were plated in 96-well plates at a density of 2×10^3/well and were cultured for 72 hours in a media containing the drugs. Cell viability was determined by using CellTiter-Glo Luminescent Cell Viability Assay (Promega, No. G7570) according to the manufacturer's instructions and measured by Envision 2104 Multi-label Microplate Reader (Perkin Elmer). Combination index (CI) was calculated by CompuSyn (26).

Western blot analysis

Cells were harvested and lysed in a NETN300 buffer [1% NP40, 300 mmol/L NaCl, 0.1 mmol/L EDTA, and 50 mmol/L Tris (pH 7.5)] containing a protease and phosphatase inhibitor cocktail (Calbiochem). Following protein concentration determination by using Bio-Rad Protein Assay Dye Reagent Concentrate solution (Bio-Rad Inc.), cell lysates were separated on reducing SDS-PAGE gels and transferred onto PVDF membranes (Millipore). Membranes were immunoblotted with phospho-ATR (T1989) (ab223258, Abcam), ATR (sc-1887, Santa Cruz Biotechnology), phospho-CHK1 (S345; No. 2348, Cell Signaling Technology), CHK1 (No. 2360, Cell Signaling Technology), phospho-RPA32 (S4/8; A300–245A, Bethyl Laboratories), RPA32 (sc-56770, Santa Cruz Biotechnology), γH2AX (05–636, EMD Millipore). The species-appropriate horseradish peroxidase (HRP)-conjugated secondary antibody was used, followed by detection with SuperSignal West Pico PLUS and Femto Chemiluminescent Substrate (Thermo Fisher Scientific). The ChemiDoc MP Imaging System (Bio-Rad) was used for image generation.

Correlation between M4344 response and RepStress and NE gene expression signatures

IC_{50} values of M4344 in 13 cancer cell lines were calculated by GraphPad Prism 7 software (GraphPad Software). The replication stress (RepStress) signature score was mined by CellMinerCDB (27), and computed as weighted sum of standardized (*Z*-score) transcript expression for the following genes: *SRSF1, SUV39H1, GINS1, PRPS1, KPNA2, AURKB, TNPO2, ORC6, CCNA2, LIG3, MTF2, GADD45G, POLA1, POLD4, POLE4, RFC5, RMI1, RRM1*. These genes encode E2F targets and G2M checkpoint and other DNA damage response components. They were selected using a combination of literature review and analyses of genes differentially expressed between small-cell lung cancer cell lines stratified by replication stress-related attributes. NE (Neuroendocrine, NE) expression signatures with 25 genes associated with NE differentiation (*BEX1, ASCL1, INSM1, CHGA, TAGLN3, KIF5C, CRMP1, SCG3, SYT4, RTN1, MYT1, SYP, KIF1A, TMSB15A, SYN1, STY11, RUNDC3A, TFF3, CHGB, FAM57B, SH3GL2, BSN, SEZ6, TMSB15B*, and *CELF3*) and 25 genes not associated with NE differentiation (*RAB27B, TGFBR2, SLC16A5, S100A10, ITGB4, YAP1, LGALS3, EPHA2, S100A16, PLAU, ABCC3, ARHGD1B, CYR61, PTGES, CCND1, IFITM2, IFITM3, AHNAK, CAV2, TACSTD2, TGFB1, EMP1, CAV1, ANXA1*, and *MYOF*; ref. 28) were mined and correlation between the signatures and IC_{50} values of M4344 was plotted with the Broad Institute Cancer Cell Line Encyclopedia (CCLE) and the Genomics and Drug Sensitivity in Cancer; Massachusetts General Hospital-Wellcome Sanger Institute (GDSC) databases by using CellMinerCDB website (http://discover.nci.nih.gov/cellminercdb; ref. 29).

Gene dependency scores for *ARID1A* and *BRG1* were mined from the Achilles project (30). Correlation analysis between IC_{50} values and gene dependency scores was plotted by using CellMinerCDB website.

Patient-derived tumor organoids

Patient-derived tumor organoids were obtained from direct needle biopsies (MB155/NCI-PC155 and MB44/NCI-PC44) at the NCI, or as patient-derived xenografts passaged in NOD SCID gamma (NSG) mice (LuCaP 145.2 and LuCaP 173.1) at the NCI and propagated *in vitro* as three-dimensional organoid cultures as described previously (31). For drug response assays, organoids were seeded at 2,000 cells/well in 384-well format in 3D-culture composed of growth factor-reduced, phenol-free Matrigel (BD Biosciences, Catalog No. 356231) mixed with prostate-specific ENR growth media (PrENR) described in ref. 32 in a ratio of 80/20%, respectively, with a final volume of 20 μL/well, and incubated at 37°C for 1 hour prior to adding an additional 30-μL media to each well. The following day, plates were dosed and allowed to grow for 1 week, with one media/drug change 72 hours after the initial dosing. At the end of the week, viability in each well was quantified using CellTiter-Glo 3D (Promega, Catalog No. G9681) according to the manufacturer's protocol.

Xenograft studies

In vivo efficacy data were generated in the human small-cell lung cancer NCI-H82 (ATCC, HTB-175) and NCI-H446 (ATCC, HTB-171) xenograft models in mice. The study design and animal usage were approved by local animal welfare authorities (Regierungspräsidium Darmstadt, protocol registration number DA4/Anz.1014). Six- to 8-week-old female CD1 nude (Crl:CD1-Foxn1^{nu}; Charles River) or H2dRag2 (C;129P2-H2d-Rag2<tm1Fwa IL2rgtm1; Taconic) mice were used for NCI-H82, and NCI-H446 studies, respectively. Mice received subcutaneous injections in the right flank with 5 million cells (in PBS/Matrigel). When tumor xenografts reached

a mean volume of 170 mm^3 (NCI-H82), or 135 mm^3 (NCI-H446), mice ($n = 10$ per treatment arm, randomized from 15 mice per arm to obtain a similar mean and median within the treatment groups) received M4344 (suspended in 15% Captisol/0.1M hydrochloride acid, pH 3.5) at a once-weekly oral dose of 10 mg/kg, Irinotecan at a once-weekly intraperitoneal dose of 50 mg/kg (Bendalis GmbH, infusion solution, 20 mg/mL stock solution, diluted in 0.9% NaCl) or the combination thereof. For the combination M4344 was applied 24 hours after Irinotecan (H82: for 2 weeks, H446: for 5 weeks). Tumor length (L) and width (W) were measured with calipers and tumor volumes were calculated using $L \times W^2/2$. Progression-free survival rate was defined as 73% increase in tumor volume from baseline according to the previous guideline (33).

Statistical analysis

Statistical analysis was calculated using two-tailed unpaired Student *t* test (for *in vitro* data) and a RM 2-way ANOVA with a Tukey multiple comparison test (for *in vivo* data) by GraphPad Prism 7 software (GraphPad Software).

Results

M4344 is a potent ATR inhibitor

M4344 is an adenosine triphosphate (ATP)-competitive inhibitor that showed minimal inhibitory activity against unrelated kinases, with at least 100-fold selectivity for ATR over 308/312 kinases tested (34). To specifically characterize the activity of M4344, we first performed cytotoxicity assays comparing M4344 with the other clinically developed other ATR inhibitors BAY1895344, berzosertib, ceralasertib, and VE-821 in DU145 prostate cancer cells (**Fig. 1A**). M4344 suppressed cancer cell proliferation at lower concentrations (**Fig. 1B**), similarly to BAY1895344 and was more potent than berzosertib, ceralasertib, and VE-821.

Because of the well-established synergism between ATR and topoisomerase I (TOP1) inhibitors (35, 36), to compare the different ATR inhibitors, we determined their effects in combination with camptothecin (CPT), a selective TOP1 inhibitor and replication stress inducer (36). Nontoxic low concentration (25 nmol/L) of M4344 strongly suppressed cell viability of prostate DU145 cancer cells in combination of CPT at nanomolar concentrations (**Fig. 1C**). BAY1895344 showed similar potency (**Fig. 1D**), but berzosertib and ceralasertib needed higher concentrations (100 nmol/L and 1 μmol/L, respectively) to achieve comparable effects (**Fig. 1E** and **F**). The differential activity of the ATR inhibitors and the potency of M4344 in combination with CPT are summarized in **Fig. 1G**.

Consistent with the potency of M4344 in cell viability assays, low dose (10 nmol/L) of M4344 and BAY189544 blocked CPT-induced activation of CHK1, a main downstream effector of ATR (**Fig. 1H**; Supplementary Fig. S1; ref. 8). Together, these results show that M4344 is a potent ATR inhibitor.

Replication stress and NE-related gene expression signatures are associated with M4344 response

Next, we examined cell viability after a single treatment with increased concentrations of M4344 in 16 cancer cell lines from various tissue types. Differential sensitivity was observed between cell lines treated with M4344 (**Fig. 2A**). Blood cancer and to a lesser degree, small lung cancer cells were most sensitive to M4344 compared with other cell lines. This might be related to higher replication stress as described in **Fig. 2C** and Supplementary Fig. S2A. Protein expression levels of relevant DNA damage response factors were correlated with response to M4344 across the 16 cell lines (**Fig. 2B**). CHK1, MSH2, and RAD51 showed positive correlations, whereas BRCA2 showed a negative correlation, consistent with the role of homologous recombination (BRCA2 and RAD51) and ATR-CHK1 in cell adaptation to replication stress.

To determine whether gene expression signatures can be predictive markers for M4344, we used a recently described replication stress (RepStress)-related gene expression signature with 18 selected genes in cancer cell models and patient tumors. We performed correlation analysis between IC_{50} values of M4344 and RepStress scores derived from the Cancer Cell Line Encyclopedia (CCLE) and Genomics of Drug Sensitivity in Cancer (GDSC) using CellMinerCDB (29). Cancer cells with high RepStress scores showed higher sensitivity than cell lines with low RepStress scores (**Fig. 2C**; Supplementary Fig. S2A).

As we recently proposed that replication stress is associated with NE phenotype in patient-derived small-cell lung cancer cell lines (27, 37), we tested the NE transcript expression signature. Supplementary Figures S2D and S2B show that cells with high NE scores were most sensitive to M4344.

Consistently, we found that the activity of ETP-46464, an ATR inhibitor, exhibited positive correlation with RepStress and NE signatures in the Cancer Therapeutics Response Portal (CTRP) database (number of cell lines: 539; Supplementary Figs. S2C and S2D). Moreover, M4344 activity showed significant correlation with gene dependency for the chromatin remodeling factors ARID1A and BRG1, consistently with recent reports describing synthetic lethality with ATR (**Fig. 2E** and **F**; refs. 18, 30, 38). Collectively, our data suggest that gene expression signatures can be exploited to predict M4344 activity in cancer therapy.

M4344 causes cell death by dysregulating replication and inducing DNA damage

To elucidate the molecular cytotoxic mechanisms of M4344, we first assessed changes of DNA synthesis in response to different concentrations of M4344 in H82 cells. EdU pulse-incorporation assays showed a biphasic response (**Fig. 2G**). At a low dose (50 and 100 nmol/L), which only produced mild cytotoxicity (see **Fig. 2A**), M4344 increased Edu incorporation, indicating unscheduled DNA synthesis, especially in the cells in late S-phase. By contrast, higher doses (500 and 1,000 nmol/L) that produced extensive cytotoxicity produced DNA synthesis collapse with reduced EdU incorporation, indicative of replication catastrophe in a large fraction of the cells throughout S-phase. Replication collapse caused by M4344 produced a strong induction γH2AX, indicative of extensive DNA damage (**Fig. 2H**).

We next accessed whether the replication stress induced by M4344 could be detected by measuring single-stranded DNA (ssDNA) in cells treated with a combination of CPT and M4344. Using immunofluorescence microscopy under nondenaturing conditions in BrdUrd-pretreated cells, we found that combination of nontoxic concentration (25 nmol/L) of M4344 with CPT led to a significant accumulation of ssDNA (Supplementary Figs. S2E and S2F). Coincidently, M4344 induced RPA32 phosphorylation (Ser4/8), an indicator of single-stranded DNA and replication stress (Supplementary Figs. S2G and S2I; refs. 39, 40). DNA damage in the nucleus of those cells with replication stress was also visualized by γH2AX induction (Supplementary Figs. S2G and S2H).

To further examine the cell death caused by M4344-induced DNA damage, we profiled the distribution of replicating cells and change of cell cycle by flow cytometry with EdU and DAPI (Supplementary Figs.

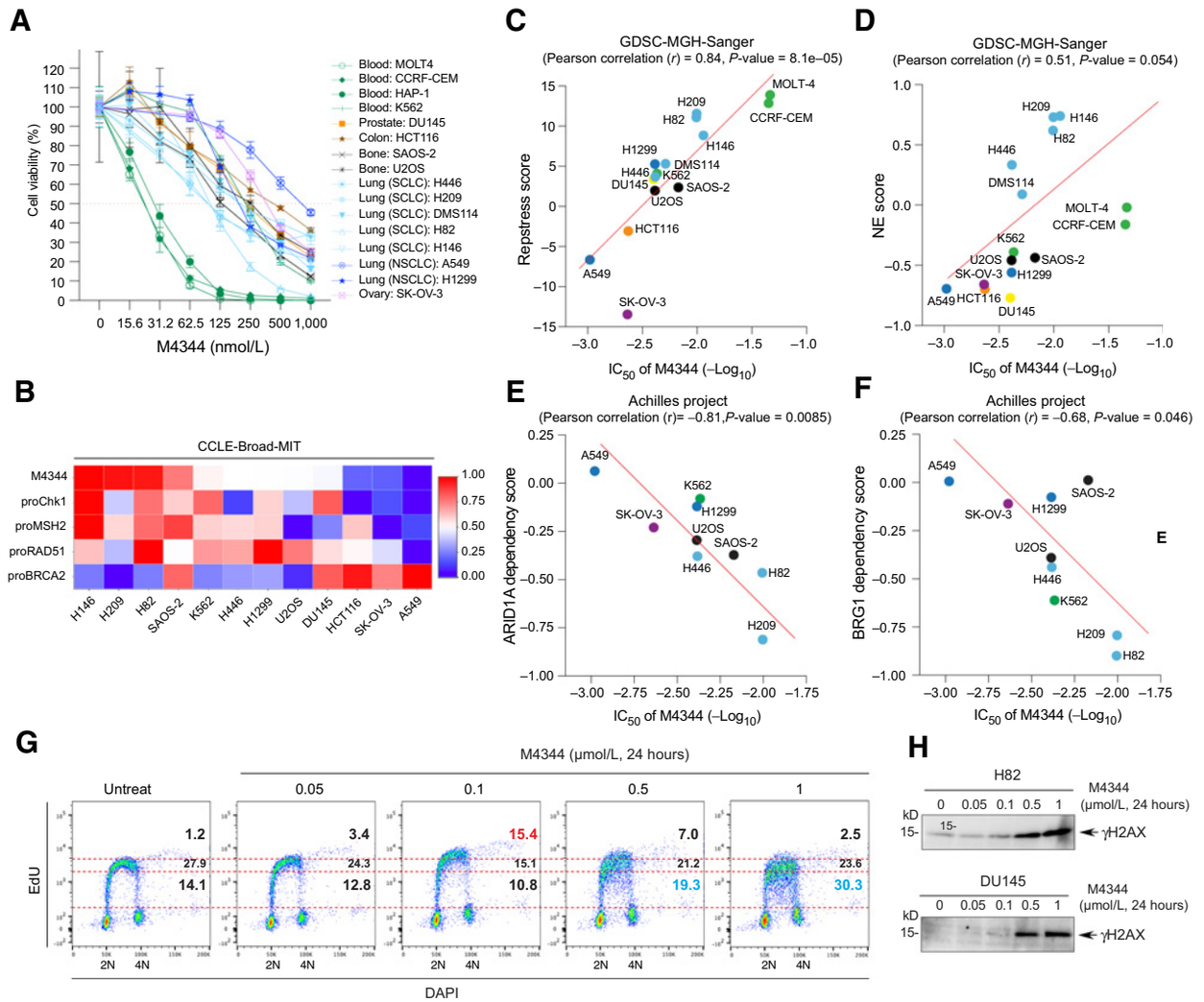

Figure 2.

M4344 kills cancer cells under replication stress (RepStress) and with NE genomic signatures by replication-mediated DNA damage. **A,** Cytotoxicity of M4344 as monotherapy in 16 cancer cell lines from different histology. Following incubation with the indicated concentrations of M4344 for 72 hours, cell viability was accessed by CellTiter-Glo assay. **B,** Correlations between protein levels related to DNA damage response pathways and M4344 sensitivity. Protein levels were mined from the CCLE cell line database. Correlation heatmap between protein levels and IC_{50} values of M4344 in **A** were generated by CellMinerCDB (http://discover.nci.nih.gov/cellminercdb). **C,** Correlation of RepStress signature scores in the GDSC databases with M4344 activity obtained in **A**. Plots were generated with CellMinerCDB. **D,** Correlation of NE signature scores in the GDSC databases with M4344 activity in **A**. Plots were generated by CellMinerCDB. **E** and **F,** Gene dependency of M4344 response. Dependency scores of ARID1A and BRG1were mined from the Project Achilles from CCLE. Plots were generated with CellMinerCDB. *P* values indicate Pearson correlation coefficients. **G,** Biphasic effect of M4344 on DNA synthesis. H82 cells treated as indicated were pulse-labeled with EdU (10 μmol/L) 30 minutes prior to harvest. Edu incorporation per cell was analyzed by FACS. Numbers indicate percentage of cells in the areas. **H,** Induction of DNA damage detected by γH2AX Western blotting. Cells were incubated with the indicated concentrations of M4344 for 24 hours.

S2J and S2K). Although CPT alone disrupted DNA replication, thereby leading to S-phase arrest, a combination of a low dose of M4344 (25 nmol/L), which alone had no detectable effect on DNA replication, completely suppressed DNA replication, resulting in fragmented cells in the sub-G_1 population and nonreplicating cells arrested in G_2–M, indicating cell death and mitotic defects, respectively.

M4344 synergizes with clinical TOP1 inhibitors

To expand the results observed with CPT (see **Fig. 1**), we tested combination treatments of M4344 with clinical TOP1 inhibitors in the NE small-cell lung cancer cell line H82 (27). We first profiled drug concentrations for combination by treatment with the DNA damaging agents alone, and then a nontoxic dose (25 nmol/L) of M4344 was selected on the basis of the **Fig. 2A**. The TOP1 inhibitors included exatecan, which is increasingly used as cytotoxin in novel antibody-drug conjugates, SN-38, the active metabolite of irinotecan, topotecan, and LMP400 (indotecan, in early clinical development; refs. 36, 41). M4344 significantly synergized with all the TOP1 inhibitors (**Fig. 3**). Exatecan showed the highest potency as a single agent, but also show significant synergy with nontoxic concentrations of M4344 in a very low nanomolar range (0.25 nmol/L; **Fig. 3A** and **E**). SN-38, the active

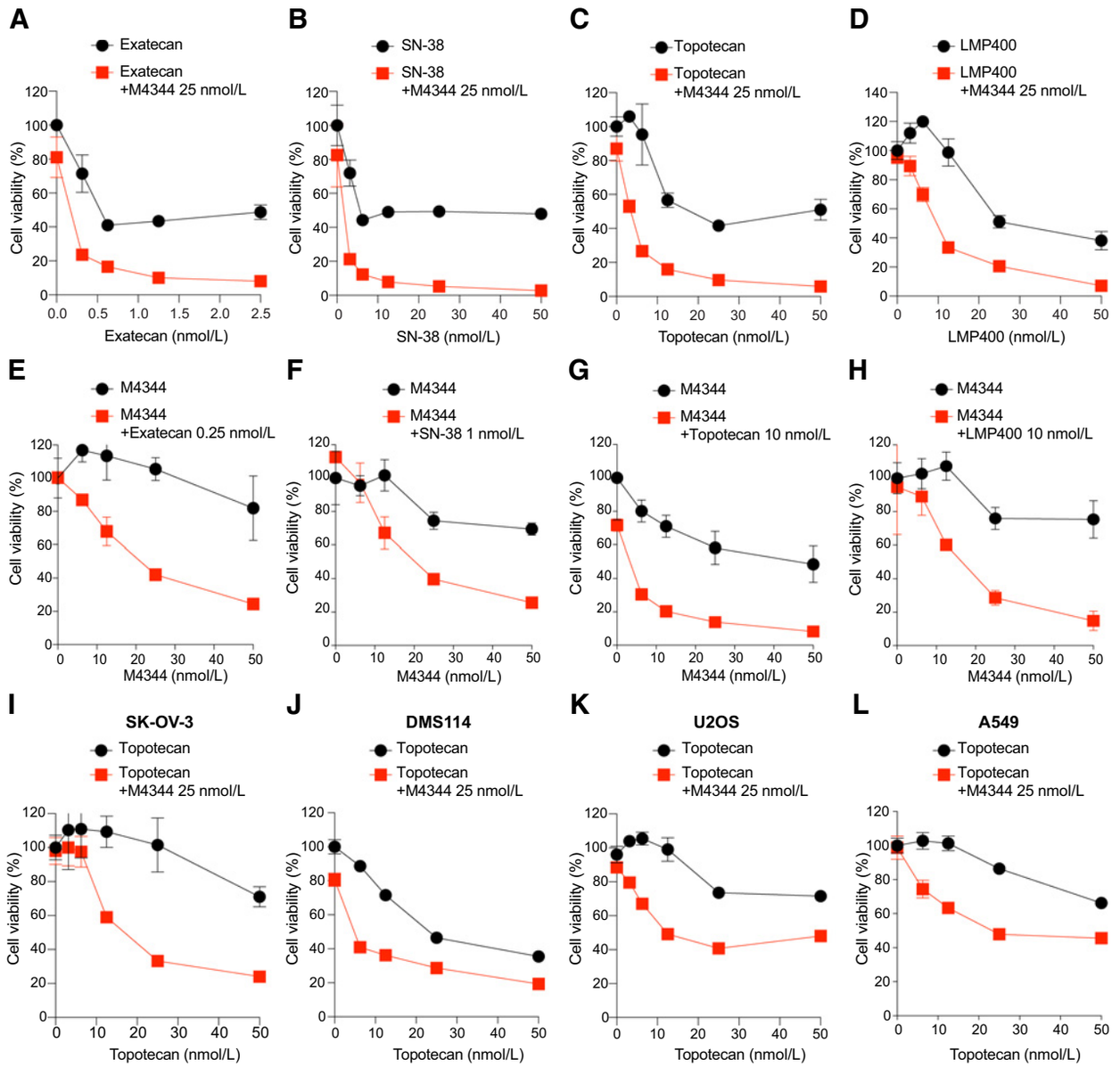

Figure 3.

M4344 synergizes clinical TOP1 inhibitors. **A–D,** H82 cells were co-incubated with M4344 (25 nmol/L) and the indicated concentrations of exatecan (**A**), SN-38 (**B**), topotecan (**C**), and indotecan (LMP400; **D**) for 72 hours. **E** and **F,** Conversely, H82 cells were co-incubated with the indicated concentrations of M4344 and exatecan (**E**, 0.25 nmol/L), SN-38 (**F**, 1 nmol/L), topotecan (**G**, 10 nmol/L), and indotecan (LMP400; **H**, 10 nmol/L) for 72 hours. **I–L,** Synergy of M4344 with topotecan in four additional cell lines: SK-OV-3 (**I**), DMS114 (**J**), U2OS (**K**), and A549 (**L**). Cells were cotreated with M4344 (25 nmol/L) and the indicated concentrations of topotecan for 72 hours. Cell viability was accessed by CellTiter-Glo assay. Synergy plots are presented in Supplementary Fig. S3.

metabolite of irinotecan also exhibited supra-additive effects with M4344 at low nanomolar range (1 nmol/L; **Fig. 3B** and **F**). Topotecan and LMP400, which required higher doses to achieve similar single-agent activity still showed synergistic effects with M4344 at 10 nmol/L dose (**Fig. 3D** and **H**). The supra-additive effects of M4344 and topotecan were extended to additional cancer cell lines: SK-OV-3, DMS114, U2OS, and A549 (**Fig. 3I–L**).

To quantify the synergistic effects observed in the combination treatments, CI values were calculated (Supplementary Fig. S3). CI values for all of the tested combinations shown in **Fig. 3** were ≤1, indicating strong synergistic effects when M4344 was combined with the four clinical TOP1 inhibitors in the five cell lines tested.

M4344 synergizes with a broad range of widely used clinical agents including etoposide, gemcitabine, cisplatin, and talazoparib

To establish the range of drugs that could be considered for combination treatment with M4344 in the clinic, we performed combination studies of M4344 in H82 cells with widely used anticancer drugs that target DNA by different mechanisms. Etoposide is a

TOP2-specific inhibitor, gemcitabine a nucleoside analogue that blocks DNA polymerase and depletes deoxyribonucleotides, cisplatin a DNA crosslinking agent and talazoparib a PARP inhibitors (42, 43). All drugs showed significant synergy with M4344 used at noncytotoxic concentrations (**Fig. 4**; Supplementary Fig. S4). These results demonstrate the potential of M4344 for combination therapy with a broad range of DNA-targeted anticancer agents.

M4344 is active in patient-derived tumor organoids and xenograft models

Next, we tested several models that are more relevant to *in vivo* activity of M4344. These included patient-derived tumor organoids from prostate cancer: the LuCaP 145.2, LuCaP 173.1, and MB155. As shown in **Fig. 5** (panels A, B, and E), two of the four organoid models, LuCaP 145.2 and LuCaP 173 showed significant enhancement of topotecan activity by noncytotoxic doses of M4344 (25 nmol/L). MB155 organoids showed only mild synergy at low doses of M4344 and topotecan (**Fig. 5C**). MB44 organoids however did not show additive response to topotecan with M4344 (**Fig. 5D** and **E**). This lack of synergy might be due the intrinsic resistance of the MB44 organoids to M4344 (Supplementary Fig. S5A) and to their intrinsic sensitivity to topotecan (**Fig. 5D**). A contributing factor could be that NE subtype organoids were more sensitive to M4344 and showed better combination effects than adenocarcinoma subtype organoids (**Fig. 5**; Supplementary Fig. S5A).

To further evaluate the efficacy of M4344 in animal tumor models, we generated H82 and H446 small-cell lung cancer cells–derived mouse xenografts and tested their response to the combination of M4344 and irinotecan. Mice were administered M4344 (10 mg/kg) and irinotecan (50 mg/kg), and subsequently tumor growth was measured. Addition of M4344 to irinotecan in both H82 and H446 xenografts led to a statistically significant decrease in tumor volume relative to single-agent therapies (**Fig. 6A** and **B**). Benefits of progression-free survival were also observed in the combination therapy over irinotecan single therapy (**Fig. 6C** and **D**). The combination was well tolerated as determined by lack of body weight (Supplementary Fig. S6). These findings indicate that M4344 effectively synergizes with TOP1 inhibitors to promote tumor suppression and regression in human cancer cells–derived experimental models.

Discussion

This study describes the molecular pharmacology of the novel ATR inhibitor, M4344 (VX-803), which is in early clinical trials. It provides insights into M4344 potency, predictive biomarkers and synergistic combinations in human cancer cell lines, and organoids and in mouse xenografts. Although several small-molecule ATR inhibitors are advancing in parallel in clinical trials, there are still unresolved questions concerning the identification and selection of groups of patients with cancer who are most likely to benefit from ATR inhibitors and how best to combine ATR inhibitors in cancer therapy. Here, we demonstrate that M4344 effectively inhibits the ATR–CHK1 pathway at nontoxic nanomolar concentrations in cancer cell lines. We report gene expression signatures as potential predictive biomarkers for

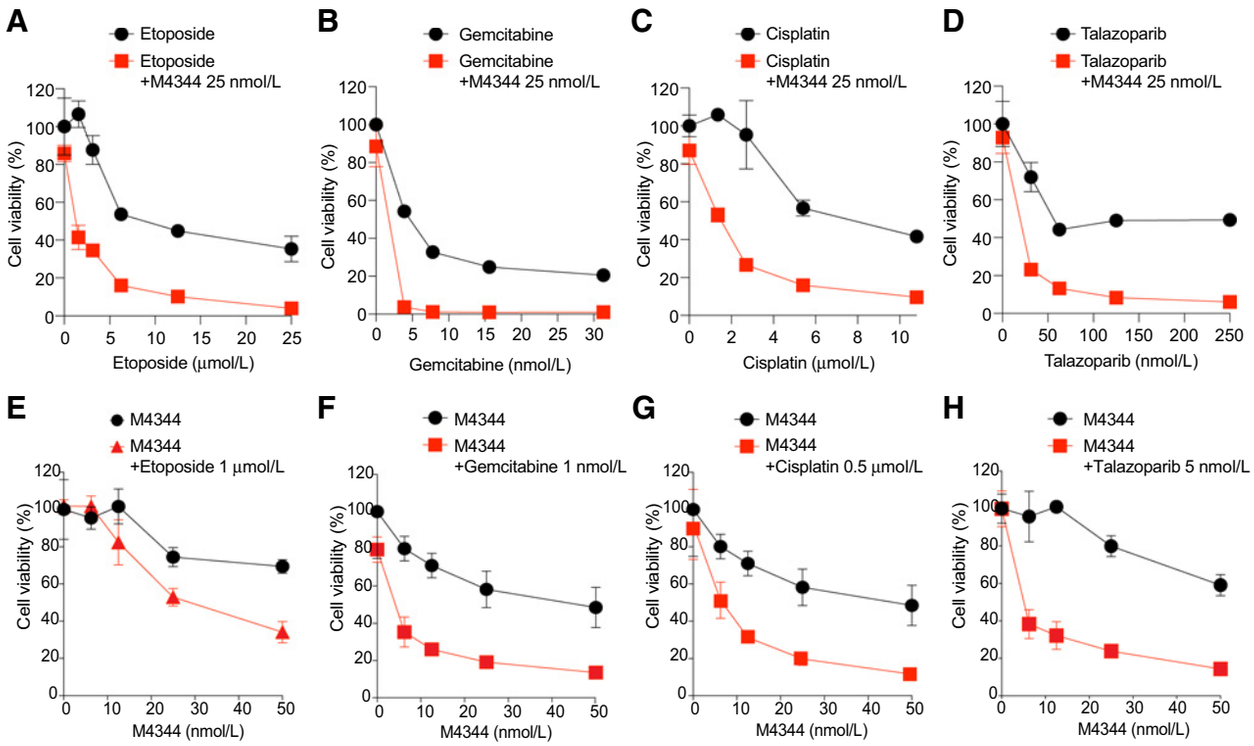

Figure 4.
M4344 shows synergy with etoposide, gemcitabine, cisplatin, and talazoparib. **A–D,** H82 cells were co-incubated with a nontoxic concentration of M4344 (25 nmol/L) and the indicated concentrations of etoposide (**A**), gemcitabine (**B**), cisplatin (**C**), and talazoparib (**D**) for 72 hours. **E–H,** H82 cells were coincubated with the indicated concentrations of M4344 and etoposide (**E**, 1 μmol/L), gemcitabine (**F**, 1 nmol/L), cisplatin (**G**, 0.5 μmol/L), and talazoparib (**H**, 5 nmol/L) for 72 hours. Cell viability was accessed by CellTiter-Glo assay. Synergy plots are presented in Supplementary Fig. S4.

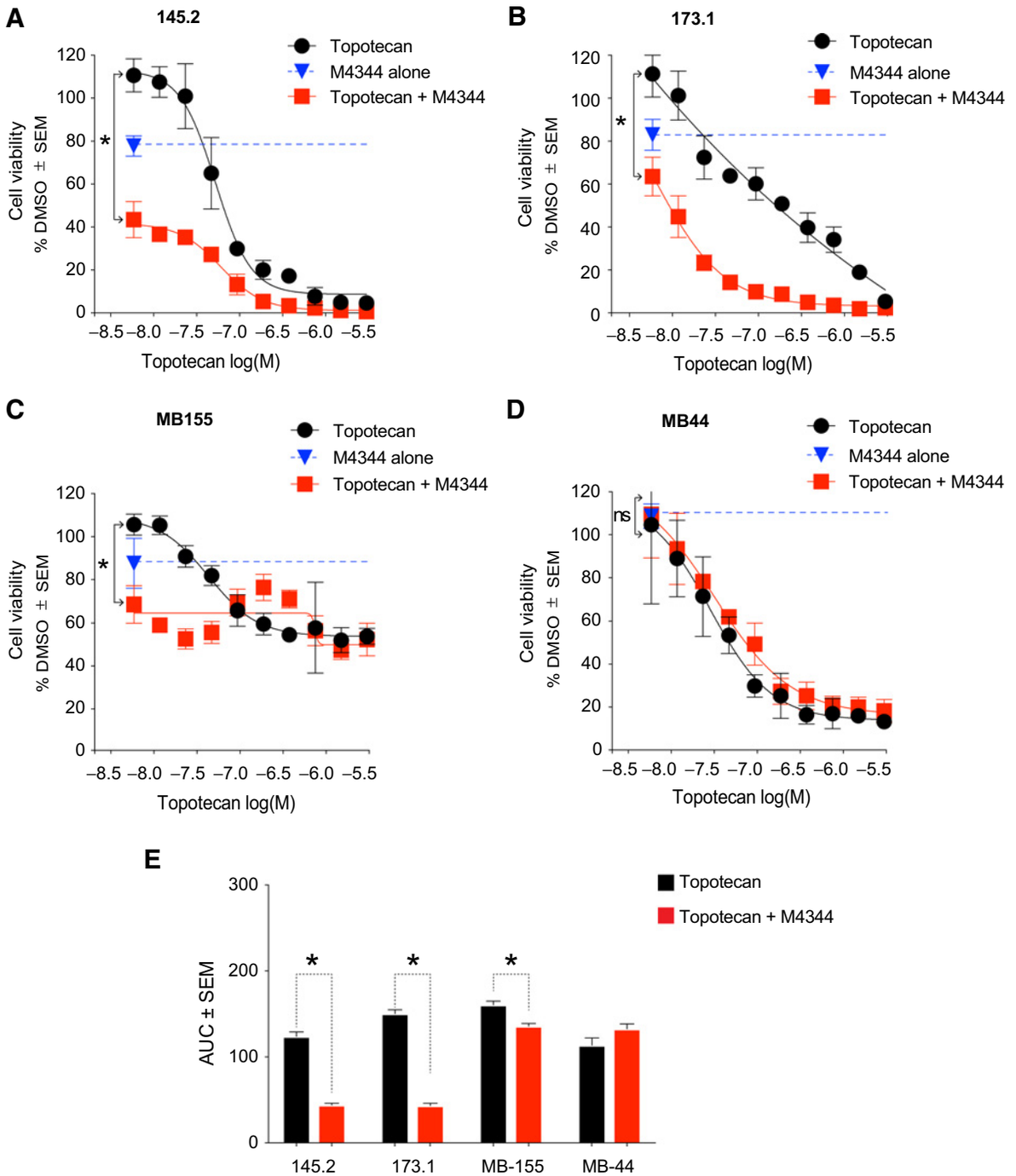

Figure 5.

M4344 synergizes with topotecan in patient derived prostate tumor organoids. **A–D,** LuCaP 145.2 (**A**), LuCaP 173.1 (**B**), MB155 (**C**), and MB44 (**D**) organoids were incubated with a noncytotoxic concentration of M4344 (25 nmol/L) and the indicated concentrations of topotecan for 72 hours. Cell viability was quantified using CellTiter-Glo 3D. Data shown are the mean ± SEM ($N = 4$ for each group). *P* values indicate statistical difference between groups (topotecan vs. combination; *, *P* values < 0.0001). **E,** Bar graph representing normalized AUC values calculated by measuring changes in cell viability of organoids treated as indicated. Data shown are the mean ± SEM ($N = 4$ for each group; *, *P* values < 0.0001).

further clinical evaluation of M4344 in cancer therapy. We also show that M4344 exhibits broad range activity in multiple cancer models as it induces significant synergy with a broad range of widely used clinical agents that target DNA and induce replication stress in various cancer cell lines, patient-derived prostate tumor organoids, and human cancer cells–derived SCLC mouse xenografts.

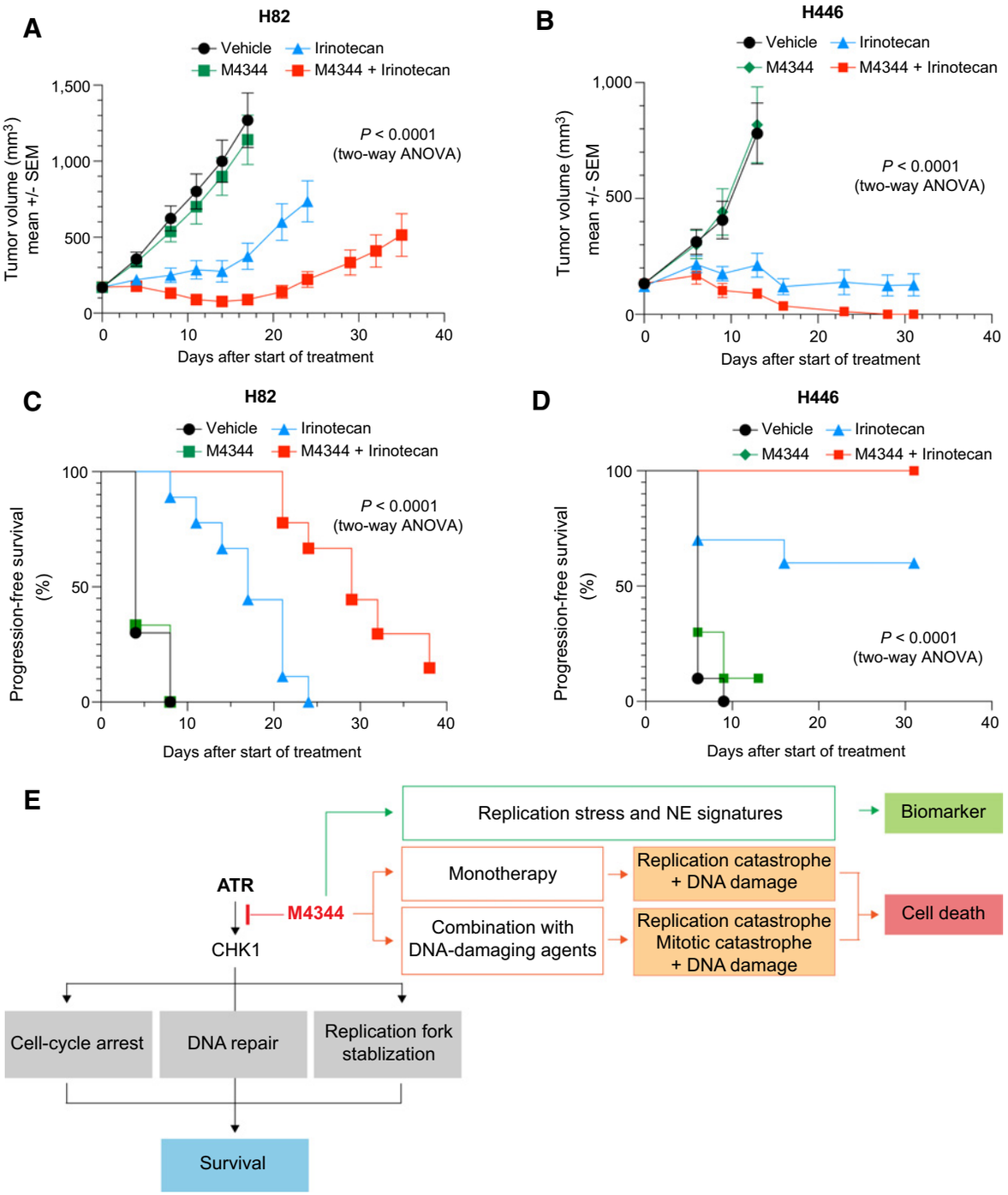

Figure 6.

Efficacy of the combination of M4344 with irinotecan in human small-cell lung cancer tumor xenografts and schematic flow chart summarizing this study. **A–D,** The *in vivo* efficacy of M4344 was evaluated in mice transplanted with H82 (**A**) and H446 (**B**) cells. Mice received subcutaneous injections in the right flank with cancer cells (in PBS/Matrigel). Mice received M4344 at an oral dose of 10 mg/kg, irinotecan at an intraperitoneal dose of 50 mg/kg or the combination thereof. Both compounds were applied once weekly, the treatment duration was 2 weeks for the H82 and 5 weeks for the H446. For the combination M4344 was applied 24 hours after Irinotecan. Tumor volumes are shown as mean ± SEM ($N = 10$ mice for each group). **C** and **D,** Benefits of progression-free survival by combination treatment, compared with control treatment and either monotherapy. **E,** M4344 inhibits activation of the ATR signaling pathway, thereby consequently blocking signal transduction from replicative DNA damage. After M43444 treatment, cells undergo replication catastrophe with DNA damage and mitotic defects, leading to cell death. Gene expression signatures including replication stress (RepStress), NE signature, and SWI/SNF inactivation are candidate predictive markers for M4344 in cancer therapy.

On the basis of single-agent cytotoxicity, synergy with TOP1 inhibitors and inhibition of CHK1 activation, we conclude that the four ATR inhibitors in clinical development can be ranked by potency as: M4344 ∼ BAY1895344 > berzosertib (M6620/VX-970) > ceralasertib (AZD6738). This ranking is consistent with recent reports and unpublished data (11, 12). It is also notable that M4344 is chemically distinct (see **Fig. 1A**), whereas berzosertib is chemically related to VE-821, itself a potent ATR inhibitor but with unsatisfactory *in vivo* activity (35), and BAY1895344 is chemically related to ceralasertib (AZD6738). Hence, further studies are warranted to compare the binding sites and molecular interactions between M4344 and ATR with the other clinical ATR inhibitors.

ATR inhibitors are being developed both as single agents and as adjuvants to chemotherapy for tumors that require ATR to adjust to replication stress and defective DNA repair (summarized in **Fig. 6E**; refs. 11, 12). Single-agent activity was clearly observed with M4344 across the 16 cell lines tested in our study as well as in two of the four prostate organoid tumors. Synthetic lethality screens with ATR have been hampered by the fact that ATR is essential in cell proliferation. Yet, siRNA screening for TOP1 inhibitors revealed ATR as synthetic lethal with CPT and LMP400 (indotecan; ref. 35). Previous reports also indicated that alterations of ATM, BRCA1/2, ARID1A, and oncogenic activation of MYC and Cyclin E1 confer hypersensitivity to ATR inhibition (reviewed in refs. 11, 12), leading to synthetic lethality. Consistent with these prior findings and the requirement for ATR to prevent replication catastrophe (**Fig. 6E**; ref. 40), our results with a gene expression signature for replication stress (RepStress) showed significant predictive values for M4344, suggesting that this RepStress signature could potentially be used to select patients for treatment with ATR inhibitors. We also confirmed the importance of dysfunctional SWI/SNF complex involved in ATR dependency by finding BRG1 (SMARCA4) dependency (38) for M4344 response in the panel of cancer cell lines examined here. Underlying the importance of chromatin structure and dynamics, we also found that inactivation of another SWI/SNF component (ARID1A), which is also commonly mutated in cancers, was significantly correlated with M4344 activity. In addition, based on the cancer cell lines and prostate organoid models, we found that tumors with NE characteristics such as SCLC (27) and prostate tumors (44) were significantly correlated with cytotoxic response to M4344. NE gene signature could be also a promising biomarker for determination of prognosis and therapeutic choice across various cancer types (45). Thus, our preclinical results may prompt further clinical studies with gene expression signatures to assess the clinical activity of M4344 and prediction of drug response, as well as expansion with other clinical ATR inhibitors (**Fig. 6E**).

As adjuvants to chemotherapy, prior studies with VE-821, berzosetib (M6620/V-970), and ceralasertib (AZD6738) have established that ATR inhibitors are highly synergistic with chemotherapeutic agents inducing replication stress (**Fig. 6E**; refs. 12, 14). Consistent with M4344 targeting ATR, we found that, in multiple models including diverse cancer cell lines, prostate organoids, and mouse xenografts, M4344 was highly synergistic with a broad range of clinically relevant replication stress inducers including TOP1 inhibitors (topotecan, irinotecan, exatecan, indotecan), PARP inhibitors (talazoparib), gemcitabine, and cisplatin. Given that those DNA damaging agents are widely used in standard of care cancer treatments, low-dose combinations of M4344 and DNA damaging agents may overcome the chemoresistance of tumors such as those with inactivation of SLFN11 (46, 47).

A challenge of combination therapies with ATR inhibitors is dose-limiting toxicity due to the fact that replicating normal tissues (intestine, bone marrow, and hair follicles) are affected by the combination in addition to the targeted rapidly proliferative tumors. One approach to spare the normal tissues is to combine ATR inhibitors with tumor-targeted TOP1 inhibitors (TTTi) using a "gapped schedule" (36). This strategy consists in administering TTTi as short intravenous infusions at broad intervals (2-4 weeks) and to give the ATR inhibitor once the normal tissues are cleared (2-3 days after the TTTi injection), on a continuous basis (daily or else depending on the pharmacokinetics of the ATR inhibitor) to ensure sustained ATR inactivation during the time the TTTi is retained in the tumor. Hence, further studies are warranted to combine M4344 orally in a gapped schedule combination with TTTis such as Enhertu and sacituzumab govitecan (36).

Another challenge is how to choose rationally among the ATR inhibitors in clinical development. Like BAY1895344 and ceralasertib, M4344 is given orally, whereas the first-generation ATR inhibitor berzosertib (M6620/VX-970) is intravenous. Although intravenous ensures reliable delivery of the drug dose to the patient, oral administrations enable continuous treatment, which would work well with "gapped scheduling." The safety, tolerability, pharmacokinetics, and pharmacodynamics of M4344 in monotherapy as well as combination with chemotherapy are being explored in a first-in-human study (NCT02278250). A clinical trial to investigate a combination of the PARP inhibitor niraparib with M4344 in PARP inhibitor resistant ovarian cancer was recently announced (NCT04149145).

In summary, M4344 is a highly potent ATR kinase inhibitor that synergizes with a broad range of clinical anticancer agents and kills cancer cells by inducing replication catastrophe, collapse of cell-cycle progression, and irreparable DNA damage (**Fig. 6E**). Our findings also raise the possibility that gene expression signature-related replication stress and NE differentiation may contribute to the selection of patients for M4344 therapy as a useful therapeutic marker.

Authors' Disclosures

A. Zimmermann is an employee of Merck KGaA, Darmstadt, Germany. A. Thomas reports grants from Merck KGa during the conduct of the study and grants from Prolynx, Tarveda, Ellipses, and AstraZeneca outside the submitted work. F.T. Zenke is an employee of Merck KGaA, Darmstadt, Germany. Y. Pommier reports grants from EMD Serono during the conduct of the study. No disclosures were reported by the other authors.

Authors' Contributions

U. Jo: Conceptualization, supervision, validation, investigation, writing–original draft. **I.S. Senatorov:** Investigation, methodology. **A. Zimmermann:** Investigation, methodology, writing–original draft. **L. Saha:** Investigation, methodology. **Y. Murai:** Investigation. **S. Kim:** Investigation, methodology. **V.N. Rajapakse:** Investigation, methodology. **F. Elloumi:** Investigation, methodology. **N. Takahashi:** Investigation, methodology, writing–original draft. **C.W. Schultz:** Investigation, methodology. **A. Thomas:** Investigation, methodology, writing–original draft. **F.T. Zenke:** Investigation, methodology, writing–original draft. **Y. Pommier:** Conceptualization, supervision, writing–original draft.

Acknowledgments

This work was supported by the Intramural Program of the Center for Cancer Research, NCI, NIH (Z01-BCC006150). Y. Pommier was supported in part by a research grant Merck KGaA, Darmstadt, Germany (M) (MCRADA 03199). We wish to thank Dr. Kathleen Kelly, head of the Laboratory of Genitourinary Cancer Pathogenesis, for her support and contribution to the prostate organoid experiments.

The costs of publication of this article were defrayed in part by the payment of page charges. This article must therefore be hereby marked *advertisement* in accordance with 18 U.S.C. Section 1734 solely to indicate this fact.

Received November 30, 2020; revised January 26, 2021; accepted May 25, 2021; published first May 27, 2021.

References

1. Jackson SP, Bartek J. The DNA-damage response in human biology and disease. Nature 2009;461:1071–8.
2. Roos WP, Thomas AD, Kaina B. DNA damage and the balance between survival and death in cancer biology. Nat Rev Cancer 2016;16:20–33.
3. Ma J, Setton J, Lee NY, Riaz N, Powell SN. The therapeutic significance of mutational signatures from DNA repair deficiency in cancer. Nat Commun 2018;9:3292.
4. Kantidze OL, Velichko AK, Luzhin AV, Petrova NV, Razin SV. Synthetically lethal interactions of ATM, ATR, and DNA-PKcs. Trends Cancer 2018;4:755–68.
5. O'Connor MJ. Targeting the DNA damage response in cancer. Mol Cell 2015;60:547–60.
6. Ubhi T, Brown GW. Exploiting DNA replication stress for cancer treatment. Cancer Res 2019;79:1730–9.
7. Blackford AN, Jackson SP. ATM, ATR, and DNA-PK: the trinity at the heart of the DNA damage response. Mol Cell 2017;66:801–17.
8. Saldivar JC, Cortez D, Cimprich KA. The essential kinase ATR: ensuring faithful duplication of a challenging genome. Nat Rev Mol Cell Biol 2017;18:622–36.
9. Karnitz LM, Zou L. Molecular pathways: targeting ATR in cancer therapy. Clin Cancer Res 2015;21:4780–5.
10. Lecona E, Fernandez-Capetillo O. Targeting ATR in cancer. Nat Rev Cancer 2018;18:586–95.
11. Gorecki L, Andrs M, Rezacova M, Korabecny J. Discovery of ATR kinase inhibitor berzosertib (VX-970, M6620): clinical candidate for cancer therapy. Pharmacol Ther 2020;210:107518.
12. Bradbury A, Hall S, Curtin N, Drew Y. Targeting ATR as cancer therapy: a new era for synthetic lethality and synergistic combinations? Pharmacol Ther 2020;207:107450.
13. Wengner AM, Siemeister G, Lucking U, Lefranc J, Wortmann L, Lienau P, et al. The novel ATR inhibitor BAY 1895344 is efficacious as monotherapy and combined with DNA damage-inducing or repair-compromising therapies in preclinical cancer models. Mol Cancer Ther 2020;19:26–38.
14. Thomas A, Redon CE, Sciuto L, Padiernos E, Ji J, Lee MJ, et al. Phase I study of ATR inhibitor M6620 in combination with topotecan in patients with advanced solid tumors. J Clin Oncol 2018;36:1594–602.
15. Yap TA, O'Carrigan B, Penney MS, Lim JS, Brown JS, de Miguel Luken MJ, et al. Phase I trial of first-in-class ATR inhibitor M6620 (VX-970) as monotherapy or in combination with carboplatin in patients with advanced solid tumors. J Clin Oncol 2020;38:3195–204.
16. Dillon MT, Boylan Z, Smith D, Guevara J, Mohammed K, Peckitt C, et al. PATRIOT: a phase I study to assess the tolerability, safety and biological effects of a specific ataxia telangiectasia and Rad3-related (ATR) inhibitor (AZD6738) as a single agent and in combination with palliative radiation therapy in patients with solid tumours. Clin Transl Radiat Oncol 2018;12:16–20.
17. Rawlinson R, Massey AJ. gammaH2AX and Chk1 phosphorylation as predictive pharmacodynamic biomarkers of Chk1 inhibitor-chemotherapy combination treatments. BMC Cancer 2014;14:483.
18. Williamson CT, Miller R, Pemberton HN, Jones SE, Campbell J, Konde A, et al. ATR inhibitors as a synthetic lethal therapy for tumours deficient in ARID1A. Nat Commun 2016;7:13837.
19. Wang C, Wang G, Feng X, Shepherd P, Zhang J, Tang M, et al. Genome-wide CRISPR screens reveal synthetic lethality of RNASEH2 deficiency and ATR inhibition. Oncogene 2019;38:2451–63.
20. Qiu Z, Fa P, Liu T, Prasad CB, Ma S, Hong Z, et al. A genome-wide pooled shRNA screen identifies PPP2R2A as a predictive biomarker for the response to ATR and CHK1 inhibitors. Cancer Res 2020;80:3305–18.
21. Dunlop CR, Wallez Y, Johnson TI, de Quirós Fernández SB, Durant ST, Cadogan EB, et al. Complete loss of ATM function augments replication catastrophe induced by ATR inhibition and gemcitabine in pancreatic cancer models. Br J Cancer 2020;123:1424–36.
22. Tan MSY, Sandanaraj E, Chong YK, Lim SW, Koh LWH, Ng WH, et al. A STAT3-based gene signature stratifies glioma patients for targeted therapy. Nat Commun 2019;10:3601.
23. Nishiwada S, Sho M, Cui Y, Yamamura K, Akahori T, Nakagawa K, et al. A gene expression signature for predicting response to neoadjuvant chemoradiotherapy in pancreatic ductal adenocarcinoma. Int J Cancer 2021;148:769–79.
24. Mazo C, Barron S, Mooney C, Gallagher WM. Multi-gene prognostic signatures and prediction of pathological complete response to neoadjuvant chemotherapy in ER-positive, HER2-negative breast cancer patients. Cancers 2020;12:1133.
25. de Klein A, Muijtjens M, van Os R, Verhoeven Y, Smit B, Carr AM, et al. Targeted disruption of the cell-cycle checkpoint gene ATR leads to early embryonic lethality in mice. Curr Biol 2000;10:479–82.
26. Zhang N, Fu JN, Chou TC. Synergistic combination of microtubule targeting anticancer fludelone with cytoprotective panaxytriol derived from panax ginseng against MX-1 cells in vitro: experimental design and data analysis using the combination index method. Am J Cancer Res 2016;6:97–104.
27. Tlemsani C, Pongor L, Elloumi F, Girard L, Huffman KE, Roper N, et al. SCLC-CellMiner: a resource for small cell lung cancer cell line genomics and pharmacology based on genomic signatures. Cell Rep 2020;33:108296.
28. Zhang W, Girard L, Zhang YA, Haruki T, Papari-Zareei M, Stastny V, et al. Small cell lung cancer tumors and preclinical models display heterogeneity of neuroendocrine phenotypes. Transl Lung Cancer Res 2018;7:32–49.
29. Rajapakse VN, Luna A, Yamade M, Loman L, Varma S, Sunshine M, et al. CellMinerCDB for integrative cross-database genomics and pharmacogenomics analyses of cancer cell lines. iScience 2018;10:247–64.
30. Tsherniak A, Vazquez F, Montgomery PG, Weir BA, Kryukov G, Cowley GS, et al. Defining a cancer dependency map. Cell 2017;170:564–76.
31. Beshiri ML, Tice CM, Tran C, Nguyen HM, Sowalsky AG, Agarwal S, et al. A PDX/Organoid biobank of advanced prostate cancers captures genomic and phenotypic heterogeneity for disease modeling and therapeutic screening. Clin Cancer Res 2018;24:4332–45.
32. Drost J, Karthaus WR, Gao D, Driehuis E, Sawyers CL, Chen Y, et al. Organoid culture systems for prostate epithelial and cancer tissue. Nat Protoc 2016;11:347–58.
33. Therasse P, Arbuck SG, Eisenhauer EA, Wanders J, Kaplan RS, Rubinstein L, et al. New guidelines to evaluate the response to treatment in solid tumors. European Organization for Research and Treatment of Cancer, National Cancer Institute of the United States, National Cancer Institute of Canada. J Natl Cancer Inst 2000;92:205–16.
34. Zenke FT, Zimmermann A, Dahmen H, Elenbaas B, Pollard J, Reaper P, et al. Antitumor activity of M4344, a potent and selective ATR inhibitor, in monotherapy and combination therapy. Cancer Res 2019;79:p.369.
35. Josse R, Martin SE, Guha R, Ormanoglu P, Pfister TD, Reaper PM, et al. ATR inhibitors VE-821 and VX-970 sensitize cancer cells to topoisomerase i inhibitors by disabling DNA replication initiation and fork elongation responses. Cancer Res 2014;74:6968–79.
36. Thomas A, Pommier Y. Targeting topoisomerase I in the era of precision medicine. Clin Cancer Res 2019;25:6581–9.
37. Thomas A, Pommier Y. Small cell lung cancer: time to revisit DNA-damaging chemotherapy. Sci Transl Med 2016;8:346fs12.
38. Gupta M, Concepcion CP, Fahey CG, Keshishian H, Bhutkar A, Brainson CF, et al. BRG1 loss predisposes lung cancers to replicative stress and ATR dependency. Cancer Res 2020;80:3841–54.
39. Shao RG, Cao CX, Zhang H, Kohn KW, Wold MS, Pommier Y. Replication-mediated DNA damage by camptothecin induces phosphorylation of RPA by DNA-dependent protein kinase and dissociates RPA:DNA-PK complexes. EMBO J 1999;18:1397–406.
40. Toledo LI, Altmeyer M, Rask MB, Lukas C, Larsen DH, Povlsen LK, et al. ATR prohibits replication catastrophe by preventing global exhaustion of RPA. Cell 2013;155:1088–103.
41. Coussy F, El-Botty R, Chateau-Joubert S, Dahmani A, Montaudon E, Leboucher S, et al. BRCAness, SLFN11, and RB1 loss predict response to topoisomerase I inhibitors in triple-negative breast cancers. Sci Transl Med 2020;12:eaax2625.
42. Murai J, Thomas A, Miettinen M, Pommier Y. Schlafen 11 (SLFN11), a restriction factor for replicative stress induced by DNA-targeting anti-cancer therapies. Pharmacol Ther 2019;201:94–102.
43. Pommier Y, O'Connor MJ, de Bono J. Laying a trap to kill cancer cells: PARP inhibitors and their mechanisms of action. Sci Transl Med 2016;8:362ps17.
44. Conteduca V, Oromendia C, Eng KW, Bareja R, Sigouros M, Molina A, et al. Clinical features of neuroendocrine prostate cancer. Eur J Cancer 2019;121:7–18.
45. Balanis NG, Sheu KM, Esedebe FN, Patel SJ, Smith BA, Park JW, et al. Pan-cancer convergence to a small-cell neuroendocrine phenotype that shares susceptibilities with hematological malignancies. Cancer Cell 2019;36:17–34.
46. Murai J, Feng Y, Yu GK, Ru Y, Tang SW, Shen Y, et al. Resistance to PARP inhibitors by SLFN11 inactivation can be overcome by ATR inhibition. Oncotarget 2016;7:76534–50.
47. Jo U, Murai Y, Chakka S, Chen L, Cheng K, Murai J, et al. SLFN11 promotes CDT1 degradation by CUL4 in DNA damage whilst its absence leads to synthetic lethality with ATR/CHK1 inhibitors. Proc Natl Acad Sci U S A 2021;118:e2015654118.